TECHNOLOGY REPORT

genesis WILEY

Generation of a new mouse line with conditionally activated signaling through the BMP receptor, ACVR1: A tool to characterize pleiotropic roles of BMP functions

Jingwen Yang[1,2] | Masako Toda Nakamura[2,3] | Shawn A. Hallett[2,4] | Hiroki Ueharu[2] | Honghao Zhang[2] | Kristen Kelley[2] | Tomokazu Fukuda[5] | Yoshihiro Komatsu[6] | Yuji Mishina[2] 🅾

[1]The State Key Laboratory Breeding Base of Basic Science of Stomatology & Key Laboratory for Oral Biomedicine of Ministry of Education, School and Hospital of Stomatology, Wuhan University, Wuhan, Hubei, 430079, China

[2]Department of Biologic and Materials Sciences & Prosthodontics, School of Dentistry, University of Michigan, MI

[3]Department of Oral Growth and Development, Fukuoka Dental College, Hakata, Fukuoka, Japan

[4]Department of Orthodontics and Pediatric Dentistry, School of Dentistry, University of Michigan, MI

[5]Department of Biological Sciences, Faculty of Science and Engineering, Iwate University, Morioka, Iwate, Japan

[6]Department of Pediatrics, University of Texas Health Science Center at Houston, John P and Katherine G McGovern Medical School Huston, TX

Correspondence
Yuji Mishina, University of Michigan, School of Dentistry, Department of Biologic and Materials Sciences & Prosthodontics, 1011 N. University Avenue, Ann Arbor, MI 48109-1078, USA.
Email: mishina@umich.edu

Funding information
National Center for Research Resources, Grant/Award Number: S10RR026475; National Institute of Arthritis and Musculoskeletal and Skin Diseases, Grant/Award Number: P30AR069620; National Institute of Dental and Craniofacial Research, Grant/Award Numbers: R01DE020843, R01DE025897

Summary

BMP signaling plays pleiotropic roles in various tissues during embryogenesis and after birth. We have previously generated a constitutively activated *Acvr1*(*ca-Acvr1*) transgenic mouse line (line L35) through pronuclei injection to investigate impacts of enhanced BMP signaling in a tissue specific manner. However, line L35 shows a restricted expression pattern of the transgene. Here, we generated another *ca-Acvr1* transgenic line, line A11, using embryonic stem (ES) transgenesis. The generated line A11 shows distinctive phenotypes from line L35, along with very limited expression levels of the transgene. When the transgene is activated in the neural crest cells in a Cre-dependent manner, line A11 exhibits cleft palate and shorter jaws, while line L35 develops ectopic cartilages and highly hypomorphic facial structures. When activated in limb buds, line A11 develops organized but smaller limb skeletal structures, while line L35 forms disorganized limbs with little mineralization. Additionally, no hetero-topic ossification (HO) is identified in line A11 when bred with *NFATc1-Cre* mice even after induction of tissue injury, which is an established protocol for HO for line L35. Therefore, the newly generated conditional *ca-Acvr1* mouse line A11 provides an additional resource to dissect highly context dependent functions of BMP signaling in development and disease.

KEYWORDS
BMP signaling, caALK2, orofacial development, palatogenesis, skeletogenesis

1 | INTRODUCTION

Bone morphogenetic proteins (BMPs) play pleiotropic roles in a context dependent manner during development and after birth (Brazil, Church, Surae, Godson, & Martin, 2015; da Silva Madaleno, Jatzlau, & Knaus, 2020; Grafe et al., 2018; Sampath & Reddi, 2020; Yang, Ueharu, & Mishina, 2020). Both loss-of and gain-of function studies for BMP signaling components revealed roles of BMPs in various types of experimental systems (Klingensmith, Matsui, Yang, & Anderson, 2010; Yang & Mishina, 2019; Zhao, 2003). Upon ligand binding, BMP receptors form hetero-multimers consisting type I and type II BMP receptors (Sanchez-Duffhues, Williams, Goumans, Heldin, & Ten Dijke, 2020; Wrana, Attisano, Wieser, Ventura, & Massague, 1994). Type II receptors then phosphorylate type I receptors within a GS box to activate the kinase activity of type I receptors, and allow them to phosphorylate downstream targets such as Smads (Wrana et al., 1994). A point mutation in the GS box of type I receptors that alters Gln (G) to Asp (D) results in the Ser/Thr kinase activity constitutively active without ligands, but in the presence of type II receptors (Bagarova et al., 2013).

ACVR1 (alternatively known as ALK2, ActRI, or ActRIA) is one of the BMP type I receptors. Homozygous null mutation of AVCRI in the mouse leads to early embryonic lethality around mid/late streak stage, suggesting its critical roles during gastrulation (Gu et al., 1999; Mishina, Crombie, Bradley, & Behringer, 1999). It has been shown that BMP signaling mediated by ACVR1 also plays a critical role in establishment of right-side identity in early mouse development (Kishigami et al., 2004) (Kishigami et al., 2004; Komatsu, Kaartinen, & Mishina, 2011), during cardiac and cartilage development (Dudas, Sridurongrit, Nagy, Okazaki, & Kaartinen, 2004; Kaartinen et al., 2004) and bone homeostasis (Kamiya, Kaartinen, & Mishina, 2011; Shi et al., 2018).

We previously reported generation of a conditional gain-of-function mouse model for ACVR1 using a constitutively activated form of ACVR1 with a mutation in the GS box (Q207D) along with the Cre-loxP system to avoid the potential lethality caused by an overdose, and ectopic BMP signaling during embryogenesis (*ca-Acvr1*, line L35) (Fukuda et al., 2006; Hu, Ueno, & Behringer, 2004). This mouse line exhibits embryonic lethality at the gastrulation stage when the transgene is activated in the epiblast, while develops heterotopic ossification (HO) when recombinant adenovirus that expresses Cre is injected to legs with cardiotoxin for tissue injury (Pan, Fleming, Hong, Mishina, & Perrien, 2020; Shimono et al., 2011; Yu et al., 2008). Meanwhile, an R206H mutation in ACVR1 was identified as a cause of Fibrodysplasia ossificans progressiva (OMIN #135100), which is a rare genetic disorder to develops HO (Shore et al., 2006).

Despite our intention to achieve ubiquitous expression of the transgene upon Cre-recombination, an expression of the line L35 is somehow restricted and augmentation of signaling levels is within several folds (Fukuda et al., 2006; Yang et al., 2021). Here, we employed a different approach to screen mouse embryonic stem (ES) cells to select clones that express high levels of the transgenic construct. Resulted mouse line showed, however, very limited expression levels of the transgene, but demonstrated distinctive phenotypes from ones developed in line L35. The conditional gain-of-function system described here provides additional resources to dissect highly context dependent functions of BMP signaling.

2 | MATERIALS AND METHODS

2.1 | Vector construction

Construction of the transgenic basic vector, CAG-Z-EGFP, was described previously (Fukuda et al., 2006). In brief, a 0.9 kb fragment of the neo cassette that contains a triple poly A signal and a 4.0-kb fragment of NTR-lacZ cassette were inserted into the EcoRV site of CAG-LITMUS28 (CAG-lacZ-LITMUS28) and a 2.5-kb fragment of IRES-EGFP cassette was further inserted to CAG-lacZ-LITMUS28. The cDNA fragment of a gene of interest can be inserted into *Pst*I site of CAG-Z-EGFP (Fukuda et al., 2006). The plasmid that contains a constitutively active form of human ACVR1 (ACVR1-Q207D, ca-AVCR1) having an HAtag at the C-terminus was kindly obtained from Dr. Takashi Imamura (Cancer Institute of Japan, Tokyo). This protein tag will allow specific detection of the transgene product at the protein level (Noda, Mishina, & Komatsu, 2016). A 1.6-kb EcoRI-XbaI fragment of ca-ACVR1 was inserted into *Pst*I site of CAG-Z-EGFP (CAG-Z-EGFP-ca-Acvr1) (Figure 1a). All ligation reactions were carried out by blunt end ligation with modification after blunt-ended reactions with T4 DNA polymerase. A single nucleotide overhang was added with Taq DNA polymerase to increase the efficiency of ligation (Marchuk, Drumm, Saulino, & Collins, 1991).

2.2 | Transgenesis and mouse breeding

One μg of the transgenic vector was linearized with *Afl*II and electroporated into 1.0×10^7 AB2.2 ES cells (Lexicon Genetics) along with linearized 0.2 μg of *Pgk-neo-bpA* (Figure 1a,b). Ninety-Six G418 resistant colonies were picked up, two replica plates were made and one was stained with X-gal for beta-galactosidase activity (Figure 1c). The other replica plates were treated with recombinant Adenovirus expressing Cre to confirm these cells were capable for Cre-dependent DNA recombination (data not shown). Two clones (A11 and D9) that showed strong beta-galactosidase activity were picked up, propagated, and injected to blastocysts obtained from C57BL6/J. The resulting chimeras were bred to C57BL6/J females and F1 agouti off spring were genotyped by PCR as described below. Both clones underwent germline and we focused on founders generated from clone A11 (line A11) since this line developed craniofacial phenotypes as described in the result section.

Following transgenic mouse strains were bred with *ca-Acvr1* line A11 mice to assess tissue-specific outcomes of augmented BMP signaling activity; *P0-Cre* (C57BL/6J-Tg(P0-Cre)94Imeg (ID 148)), *Prrx1-Cre*, (Tg[Prrx1-cre]1Cjt), and *NFATc1-Cre* (Ntatc1[tm1.1[cre]Bz]) (Logan et al., 2002; Wu et al., 2012; Yamauchi et al., 1999). For tissue injury, 0.9 μg of cardiotoxin (L8102, Latoxan) dissolved in 10 μl of phosphate buffered saline was injected per leg.

All mouse experiments were performed in accordance with institutional guidelines covering the humane care and use of animals in
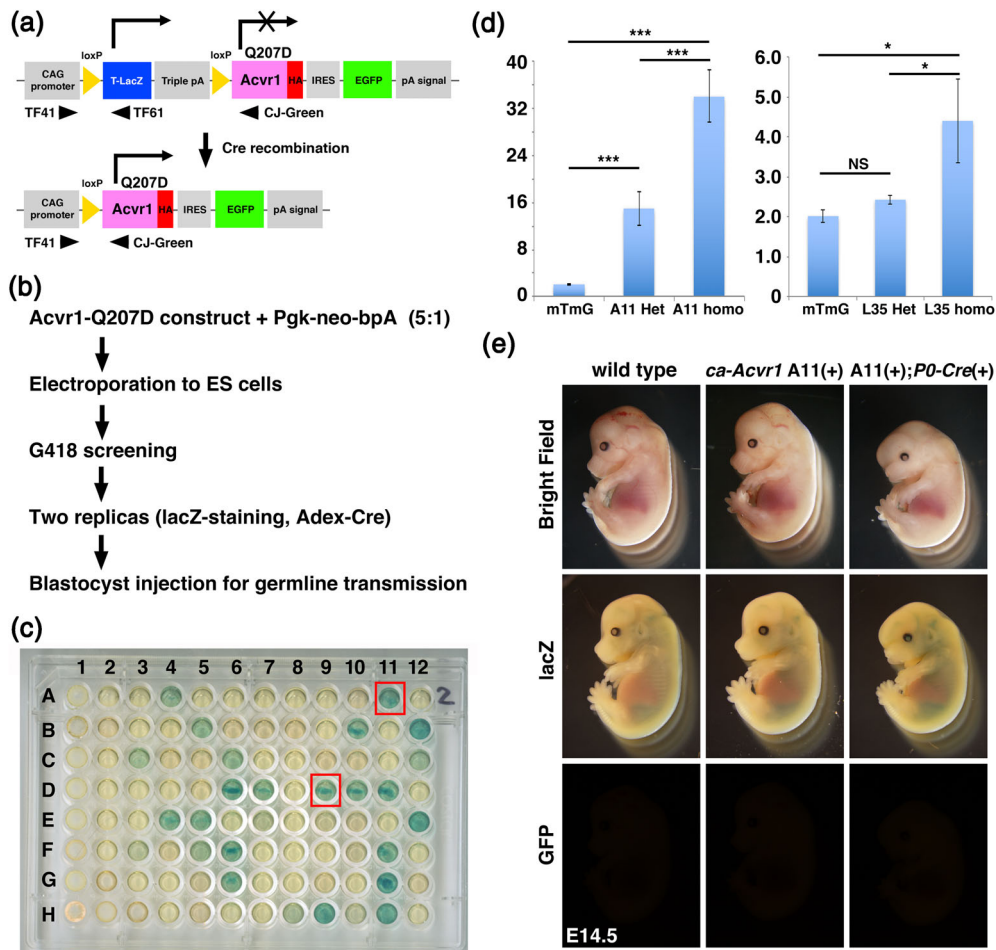
FIGURE 1 Generation of constitutively activated ACVR1 mouse line and initial characterization. (a) A concept of the transgenic construct. Human ACVR1 cDNA with the Q207D mutation was ligated with IRES-EGFP and also ligated with the CAG promoter but intercepted by a floxed *lacZ* cassette with triple polyA sites. Cells with this transgenic construct are expected to generate beta-galactosidase from the *lacZ* cassette. Cre-dependent DNA recombination removed triple polyA sites to generate ACVR1 with Q207D protein (constitutively activated ACVR1, ca-ACVR1) and to produce GFP fluorescence. Approximate positions of three PCR primers for genotyping are shown. Sequence information of those primers are shown in Table S1. (b) Screening strategy. The linearized transgenic construct was electroporated into ES cells with a Pgk-neo selection vector. Ninety eight G418-resistance clones were picked up and examined their beta-galactosidase activity and capability to recombination capability by Cre. (c) lacZ staining results. Replicated cells were stained with X-gal. Two clones that showed strong signal, A11 and D9, were further propagated and injected to blastocysts for germline transmission. (d) Quantitative genomic PCR for copy number estimation. Homozygous mice for mTmG are used as a control (1 copy of EGFP per haploid). $n = 3$. Sequence information of TaqMan primers are shown in Table S2. (e) Initial characterization of *ca-Acvr1* line A11. After breeding with P0-Cre mice, embryos were harvested at E14.5. After observation of EGFP, embryos were stained with X-gal. Littermates who did not have both transgenes were used as wild type

research. The animal protocols were approved by the Institutional Animal Care and Use Committees at the National Institute of Environmental Health Sciences (while T. F., Y. K., and Y. M. were affiliated) and the University of Michigan. The authors are current exploring possibilities to deposit the newly developed mice to public repositories and are happy to share them upon request.

2.3 | Genomic PCR and genomic Q-PCR

Genotypes were determined by genomic PCR. Sequences for each primer were shown in Table S1. For the Cre transgene, we used Cre F and Cre R of which target size is 696-bp, and for the *ca-Acvr1* transgene we used TF41 and TF61 of which target size is 580-bp (Figure 1a). CJ-Green was used along with TF41 to detect Cre induced DNA recombination (the target size; ~350-bp). Primers for the endogenous genes were used as internal controls as follow; *Alk2/Acvr1* locus for Cre: A2-5 and A2-3 (the target size is 330-bp), *Evc2/Limbin* locus for caAlk2: LbnFR1 and LbnRev3 (the target size; 334 bp), and *Tak1* locus for Cre-recombined *ca-Acvr1*: TAK1 G1 and TAK1 G2 (the target size is 200-bp) (Liu et al., 2018; Zhang et al., 2015). Genomic real-time quantitative PCR was performed using TaqMan Gene Expression Assays to quantify copy numbers of the *Egfp* cassette with a custom designed TaqMan primer set (Table S2). A TaqMan primer

set for *Gapdh* (Mm99999915_g1, cat# 4351368) was used for an internal control. Homozygous mice for mT/mG Cre reporter mice (*Gt (ROSA)26Sor*^tm4(ACTB-tdTomato,-EGFP)Luo) were used as a reference (two copies per animal) (Muzumdar, Tasic, Miyamichi, Li, & Luo, 2007).

2.4 | Micro computed tomography evaluation

Whole heads from E18.5 embryos were dissected, fixed with 70% ethanol, and then scanned using a micro computed tomography (μCT) system (μCT100 Scanco Medical, Bassersdorf, Switzerland). Scan settings were voxel size 10 μm, medium resolution, energy 70 kV, intensity 114 μA, 0.5 mm AL filter, and integration time 500 μs. Analysis was performed using the manufacturer's software. 3D models of embryos were reconstructed through MicroView (http://www.parallax-innovations.com/microview.html).

2.5 | Histology, cartilage staining, and skeletal staining

Embryos were fixed in 4% paraformaldehyde (PFA), embedded in paraffin, sectioned, and stained with hematoxylin and eosin (H&E) or Safranin O & Fast Green according to a standard procedure. For cardiac observations, embryos at E14.5 were immersed in 30% sucrose in phosphate buffered saline (PBS) after PFA fixation, then, embedded in optimal cutting temperature (OCT) compound (Fisher Healthcare). Serial transverse sections were prepared with 10 μm thickness subjected for H&E staining. For whole cartilage staining, embryos were fixed with Bouin's solution, stained with alcian blue and cleared with 1:1 mixture of benzyl benzoate and benzyl alcohol (Jegalian & De Robertis, 1992). For skeletal staining, skinned pups were stained with alcian blue and alizarin red (Hayano, Komatsu, Pan, & Mishina, 2015).

2.6 | Western blot analyses

For protein extraction, harvested embryonic tissues were washed with PBS containing a protease inhibitor cocktail (Roche) and homogenized in NP40 lysis buffer (20 mM pH 8.0 Tris–HCl, 137 mM NaCl, 1% NP40, 10% Glycerol, 1 mM Na3VO4) using a Bio-Gen Pro200 homogenizer (Pro Scientific, Oxford, CT). Sodium dodecyl sulfate-polyacrylamide gel electrophoresis (SDS-PAGE) and Western blot were carried out according to standard protocol. Antigen detection was performed using antibodies directed against total Samd1 (9743S, Cell signaling Technology), P-Smad1/5/9 (13820, Cell signaling Technology) and glyceraldehyde 3-phosphate dehydrogenase (GAPDH; 5,174, Cell Signaling Technology). Bound primary antibodies were detected with horseradish peroxidase-conjugated species-specific secondary antibodies (Cell signaling Technology) and the immunoreactive bands were quantified using ImageJ. The mean ratios of the indicated protein from three independent experiments are shown on the right of the figures.

2.7 | Statistical analyses

Morphometric measurements were made using ImageJ 1.50i (NIH) at defined anatomical landmarks. Statistical analyses were performed using Prism. All values were expressed as mean ± *SD* ANOVA were used to analyze the differences between or among groups. A *p*-value of less than .05 was considered statistically significant. All representative experiments shown were repeated three or more times. Experiments and analyses were performed in a blinded manner.

3 | RESULTS AND DISCUSSION

To generate conditional constitutively active (ca) *Acvr1* transgenic mice, we used *CAG-Z-EGFP* vector that is the same transgenic construct previously used to generate a transgenic line through pronuclei injection (line L35) (Figure 1a) (Fukuda et al., 2006; Fukuda, Mishina, Walker, & DiAugustine, 2005). A CAG promoter was used for ubiquitous expression and a *lacZ* with a nuclear translocation signal was used for detection of transgene expression. The *lacZ* cassette followed by a triple polyA signal site was floxed to allow Cre-dependent production of ACVR1 (aka Activin receptor like kinase 2, ALK2) with a Q207D gain-of-function mutation. An IRES-EGFP cassette was used to monitor Cre-dependent activation of the transgene. Here, we took an advantage of ES transgenesis to screen ES cell clones that highly express the transgene before generation of chimeric mice. The linearized transgenic vector was electroporated to AB2.2 ES cells with a *Pgk-neo-bpA* selection cassette and G418 resistant colonies were picked up to detect their beta-galactosidase activity (Figure 1b,c). We selected two clones (A11 and D9) that showed strong X-gal staining and injected to blastocysts. Both clones underwent germline, however, unexpectedly, neither line showed any X-gal staining. Because the line A11 developed craniofacial phenotypes as described below, we further analyzed line A11. In this report, we also compared phenotypes with line L35 *ca-Acvr1* transgenic mouse line we generated some years ago through pronuclei injection using the same transgenic vector (Fukuda et al., 2006).

First, we quantified the copy number of the transgene in line A11 *ca-Acvr1* transgenic mice using genomic quantitative real-time PCR. Both lines were maintained for several years in our colony and bred more than 20 generations, suggesting that each mouse line has one integrated locus per haploid. We used homozygous mT/mG mice (Muzumdar et al., 2007) as a standard (two copies per animal) to quantify copy number of *Egfp*. Results showed that heterozygous mice have 16 copies per animal while homozygous mice have 32 copies per animal suggesting that 16 copies of the transgenic cassette were integrated into one locus in the genome (Figure 1d). Similar analyses were done for line L35 suggesting that two copies of the transgenic cassette were integrated per locus in this line (Figure 1d). The mice used for quantitative PCR were subsequently bred with wild type mates to genetically confirm their genotypes as either heterozygous or homozygous for the transgene (data not shown). Homozygous mice either for line L35 or line A11 *ca-Acvr1* mice are normal, healthy and fertile with a normal litter size.

We next bred the line A11 mice with *P0-Cre* transgenic mice that expresses Cre in a neural crest-specific manner (Chen et al., 2017; Suzawa et al., 2020; Yamauchi et al., 1999). Unlike expected embryos that carry the *ca-Acvr1* transgenic construct were negative for beta-galactosidase activity (Figure 1e, middle row). Embryos that carry both the transgenic construct and *P0-Cre* transgene were negative for green fluorescence either (Figure 1e, bottom row). These results suggest that even when we selected ES cell clones that highly expressed beta-galactosidase, expression of the transgene was down regulated during ES transgenesis. However, embryos carrying both *ca-Acvr1* and *P0-Cre* transgenes showed abnormal craniofacial development (Figure 1e, right column) suggesting that very limited expression of *ca-Acvr1* from the transgenic locus is sufficient to increase BMP signaling leading to developmental abnormalities.

We then set up timed mating to follow morphological changes of line A11 *ca-Acvr1* embryos along with line L35 *ca-Acvr1* embryos. For line L35 *ca-Acvr1* mice bred with P0-Cre mouse line (*ca-Acvr1*(+):P0-Cre(+), L35 mut hereafter), they were relatively normal while showing a smaller nasal processes at embryonic day 10.5 (E10.5) (Figure 2a). The deformed maxillary and nasal regions were observed as early as at E13.5 (Figure 2a, middle row). A bulge-like structure in the forehead became obvious from E15.5. The mutant embryos also developed deformed lips. None of the L35 mut was able to survive after birth (*n* > 40). For line A11 *ca-Acvr1* mice bred with *P0-Cre* mouse line, (*ca-Acvr1*(+):P0-Cre(+), A11 mut hereafter), there were no overt morphological changes at E10.5 except showing a smaller nasal processes (Figure 2a). Like L35 mut, hypomorphic facial processes were recognized as early as at E13.5 (Figure 2a, bottom row). However, contrasting to L35 mut, the size of the frontal region of A11 mut is comparable with that of control (E17.5 lateral view). Approximately 90% of the A11 mut was not able to survive after birth (*n* > 40).

FIGURE 2 Neural-crest specific augmentation of BMP signaling via ACVR1-Q207D develops distinctive phenotypes in two transgenic lines. (a) Lateral views of the head region of control and two transgenic lines during mid to late gestation, and newborn stages. Bar =1 mm. (b) Assessment of skeletal abnormalities at E18.5 through Alcian blue/alizarin red staining (left) and microCT (right). (c) Genomic PCR to confirm genotypes of each embryo. Primers used; Cre F and Cre R (top), TF41 and TF61 (middle), and TF41 and CJ-Green (bottom) to detect presence of *Cre*, *ca-Acvr1*, recombined *ca-Acvr1*, respectively. (d) Protein lysates were prepared from E10.5 embryos and BMP-Smad levels were measured by western blots using antibodies against total Smad1 and pSmad1/5/9. Levels of signals were normalized by GAPDH. *, *p* < .05. L35 mut, *ca-Avcr1* line 35 embryos (Fukuda et al., 2006) also carrying P0-Cre transgene. A11 mut, *ca-Avcr1* line A11 (this study) embryos also carrying P0-Cre transgene
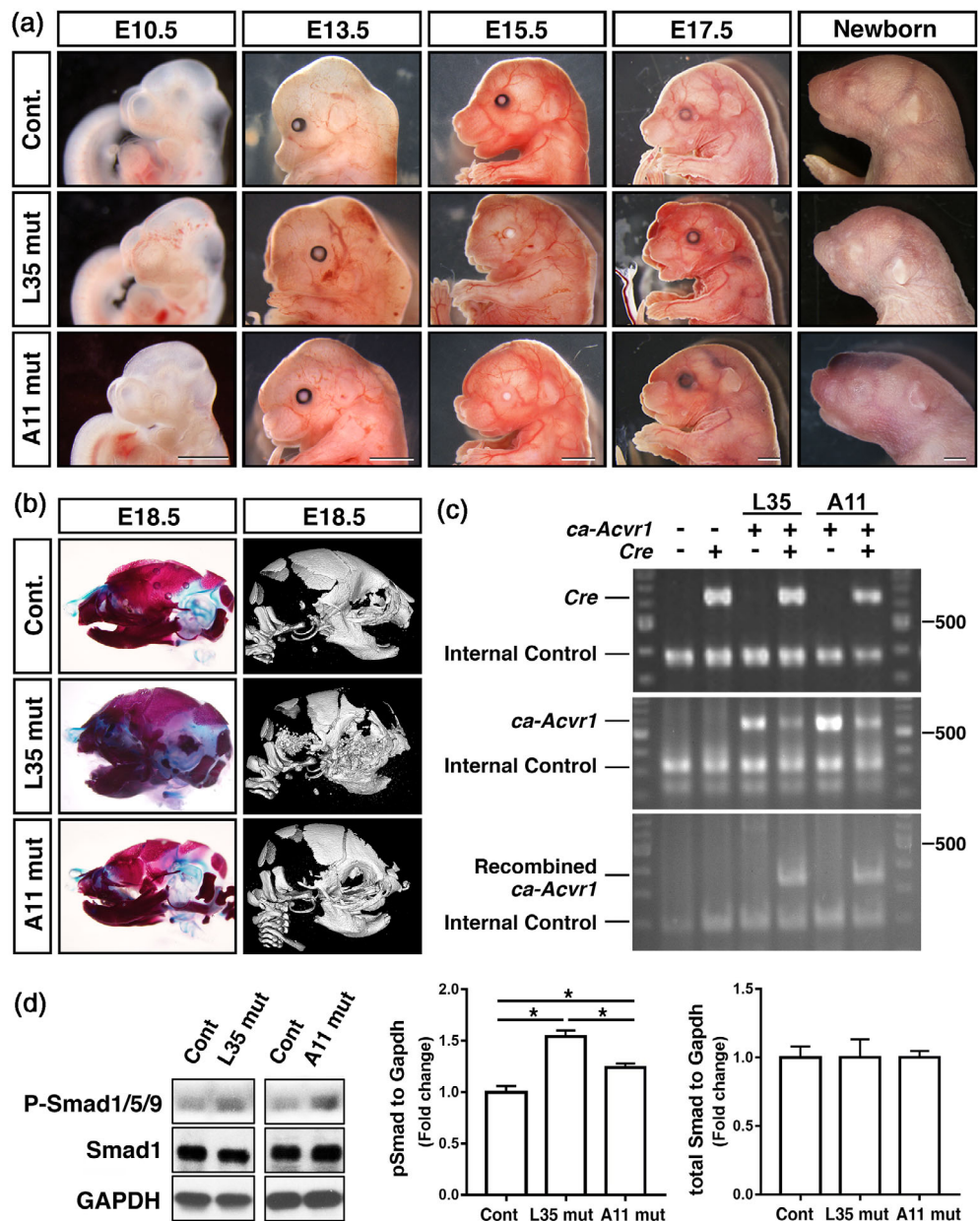
Next, we examined morphological changes in cranial skeletogenesis. Alcian blue—alizarin red staining as well as microCT images revealed that L35 mut developed a shorter skull and highly hypomorphic nasal bones and mandibles. Frontal bones and maxilla were hypo-mineralized (Figure 2b). For A11 mut, overall skeletal structure was comparable to that of controls, but they developed shorter maxillae and mandibles (Figure 2b).

Embryos carrying both the *P0-Cre* transgene and the *caAcvr1* transgene showed Cre-dependent recombination evidenced by PCR amplification of the expected size of band (∼350-bp) for both line L35 and line A11 (Figure 2c). Levels of BMP signaling activity was measured by quantification of phospho-Smad1/5/9 (P-Smad1/5/9) using protein lysate prepared from frontal heads of E10.5 embryos including the nasal process and branchial arches. Both line L35 and A11 samples showed significantly higher levels of BMP-Smad signaling compared with controls, but L35 showed more robust augmentation (Figure 2d). These facts may explain, at least in part, more severe craniofacial phenotypes developed in L35 mut depicted in Figure 2.

To gain insight how these structure abnormalities developed, we looked at several stages of embryos. Histologic observation revealed that in L35 mut at E13.5 the palatal shelves were formed but smaller than those in controls (Figure 3 top). In contract, A11 mut developed comparable palatal shelves at E13.5 with these in controls (Figure 3 top). Tongue and Meckel's cartilage developed normally at this stage in A11 mut (Figure 3 top). At E15.5, the palatal shelves in A11 mut were shorter and remained unfused (Figure 3, middle). Similar palatal structural abnormalities were observed at E17.5 along with a deformed tongue in A11 mut (Figure 3, bottom). Palatal shelves in L35 remained small at E15.5 and 17. 5, and did not fuse (Figure 3, middle and bottom).

Histologic observation of L35 mut revealed abnormal tissue condensations in the tongue and surrounding tissues (Figure 3, middle column) indicating formation of ectopic cartilage as we recently reported (Yang et al., 2021). We stained the tissues with Safranin O and fast green to confirm formation of ectopic cartilage in L35 mut while the Meckel's cartilage was hypomorphic (Figure 4a,b, middle
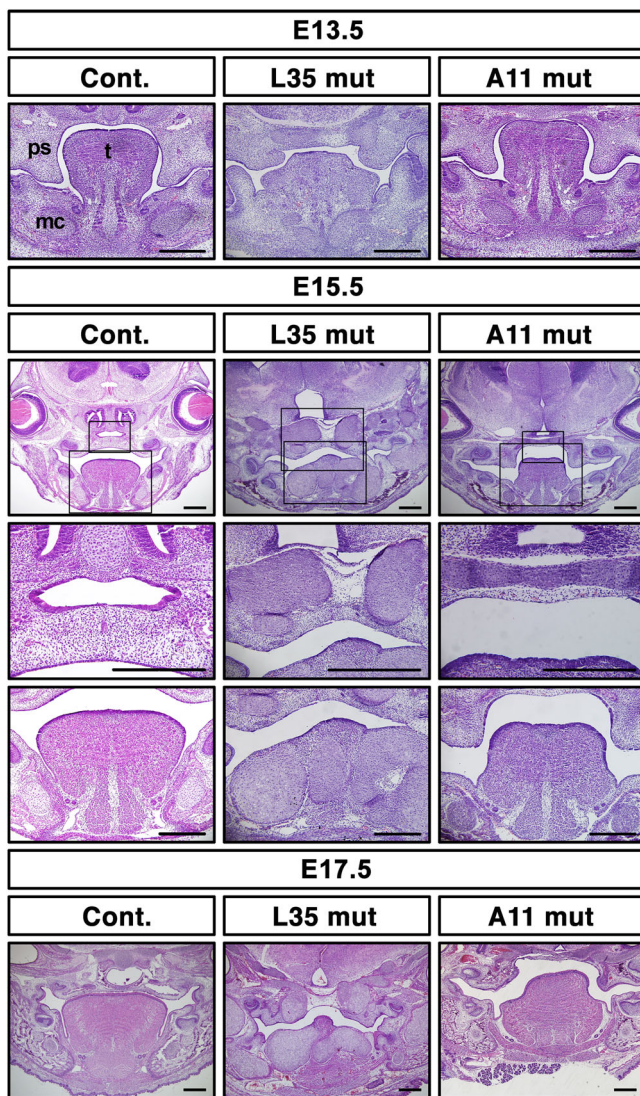

FIGURE 3 Abnormal palatogenesis in A11 mut embryos. Frontal sections at eye levels were made from control and two mutant lines of embryos at the indicated stages and stained with hematoxylin and eosin. For E15.5 samples, enlarged images for the palate and the tongue, respectively, are also shown. mc, Meckel's cartilage, ps, palatal shelf, t, tongue. Bar = 200 μm
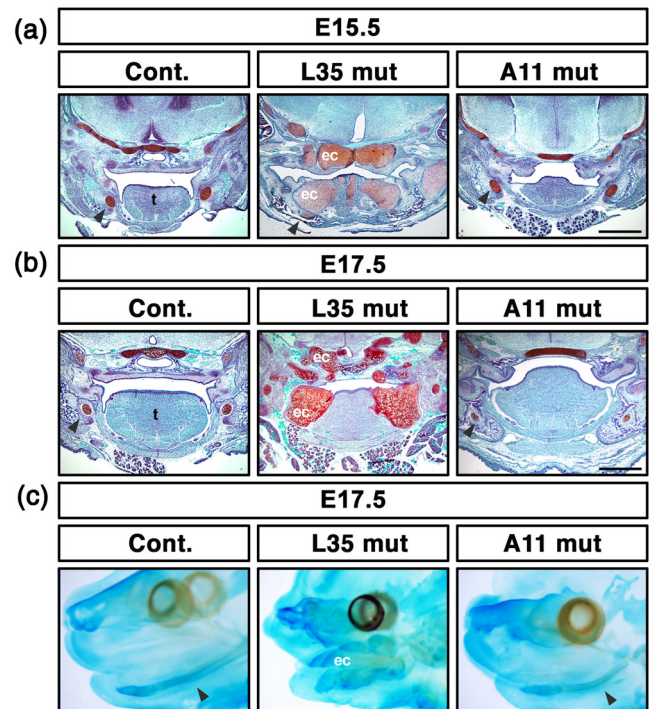

FIGURE 4 Ectopic cartilage formation in L35 mut embryos, but not in A11 mut embryos. (a, b) Frontal sections at eye levels were made and stained with safranin O (red) and counterstained with Fast Green (blue) at E15.5 or E17.5. Formation of massive ectopic cartilage is visualized in L35 mut embryos. Bar = 500 μm. (c) Whole mount alcian blue staining at E17.5. Arrowheads, Meckel's cartilage, ec, ectopic cartilage, t, tongue

column). In contrast, no ectopic cartilage was identified in A11 mut embryos (Figure 4a,b, right column). Whole mount cartilage staining at E17.5 confirms this notion, that is, massive ectopic cartilage was developed in L35 mut embryos with undistinctive Meckel's cartilage, while abnormal shaped nasal cartilage and shorter Meckel's cartilage were identified in A11 mut embryos (Figure 4c).

Because BMP signaling play an important role in cardiac neural crest cells as we and others reported that conditional disruption of type 1 BMP receptors in neural crest cells results in defects in outflow tracts and volve function (Kaartinen et al., 2004; Morikawa et al., 2009; Nomura-Kitabayashi et al., 2009; Stottmann, Choi, Mishina, Meyers, & Klingensmith, 2004), we sought potential phenotypes in cardiac tissues in these two mutant lines. Histologic observation at E14.5 revealed that abnormally shaped superior atrioventricular cushions (SAC) in one of five A11 mut embryos (Figure 5o,p). L35 mut embryos showed comparable morphology with control embryos (Figure 5a–h, n = 3 for each). SAC is known to be neural crest origin (Jiang, Rowitch, Soriano, McMahon, & Sucov, 2000), thus it is likely this abnormality is caused by increased BMP signaling in this tissue.

Next, we bred both lines with *Prrx1*-Cre transgenic line (Logan et al., 2002) to evaluate a potential difference of the two lines in limb mesenchyme. At E10.5, formation of both forelimb buds and hindlimb buds in A11 mutant embryos were comparable with these in littermate controls (Figure 6A,C), while nearly no signs of forelimb buds were identified in L35 mutant embryos (Figure 6B). At E14.5, control embryos established distinctive limb structures (Figure 6E1, autopod (a), zeugopod (b), stylopod (c) and scapula (d) for forelimbs, and autopod (e), zeugopod (f), and stylopod (g) for hindlimbs. In L35 mutant embryos, cartilage primordia were highly disorganized in both types of limbs with a greater degree in forelimb buds (Figure 6F,G, G1). At E15.5, L35 mut embryos showed very little mineralization in the appendicular bones and became necrotic by E17.5 (Figure S1). In A11 mutant embryos, cartilage primordia were relatively normal at E14.5 (Figure 6H,I,I1). A11 mutants were able to survive postnatally, however, skeletal components in arms and legs were significantly smaller than those in littermate controls at postnatal day 20 (PN20, Figure 6J,K). Because body sizes of A11 mutant mice were smaller, we normalized the length of each segment of appendicular bones by
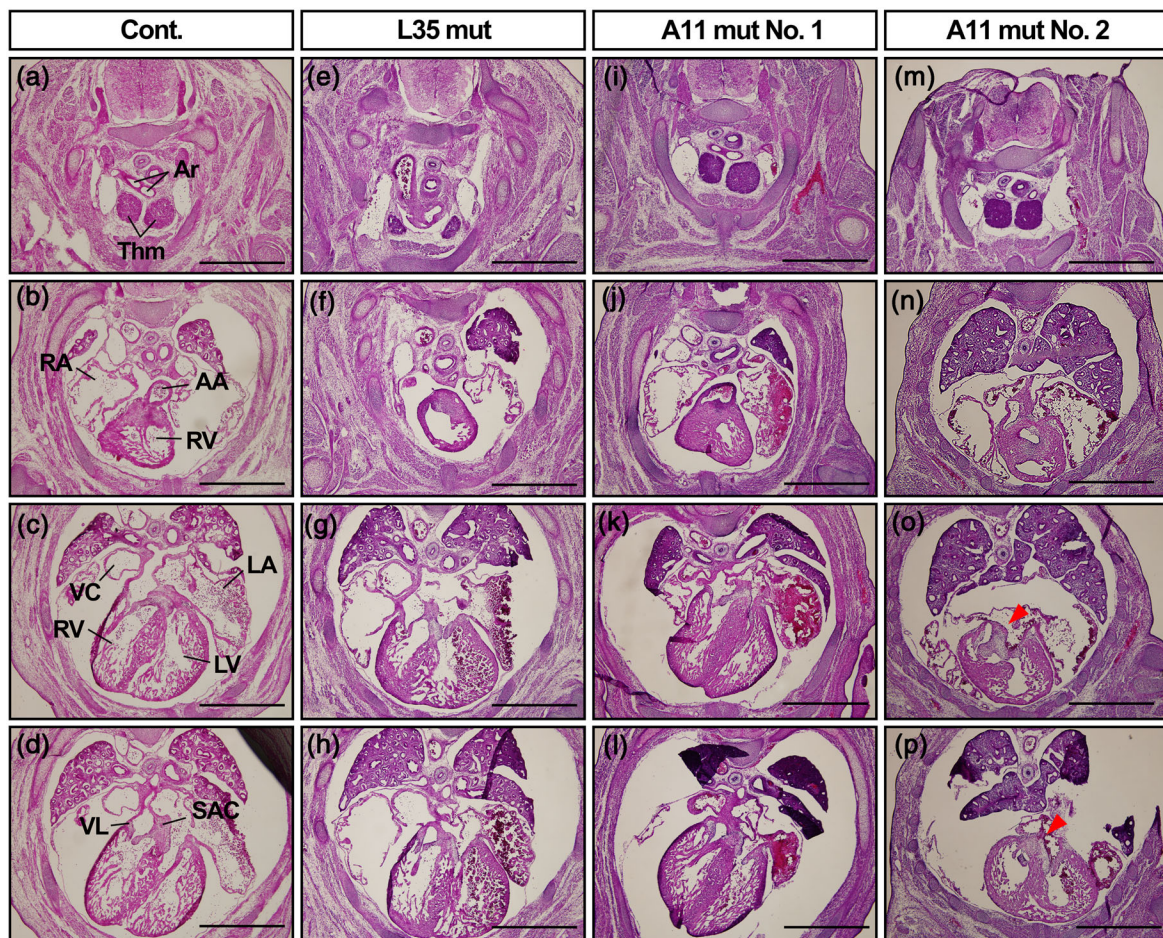

FIGURE 5 Abnormal cardiac development in A11 mut embryos but not in L35 mut embryos. Serial transverse sections for the cardiac part of control and two mutant lines of embryos at E14.5 were prepared and stained with hematoxylin and eosin. N = 3 for controls and L35 mut, and n = 5 for A11 mut. Two A11 mut embryos are shown. Arrowheads, an abnormal cushion tissue in A11 mut embryo. Ar, artery, Thm, thymus, AA, ascending aorta, RA, right atrium, RV, right ventricle, LA, left atrium, LV, left ventricle, VC, vena cava, VL, valve leaflet, SAC, superior atrioventricular cushion tissue. Bar = 1 mm
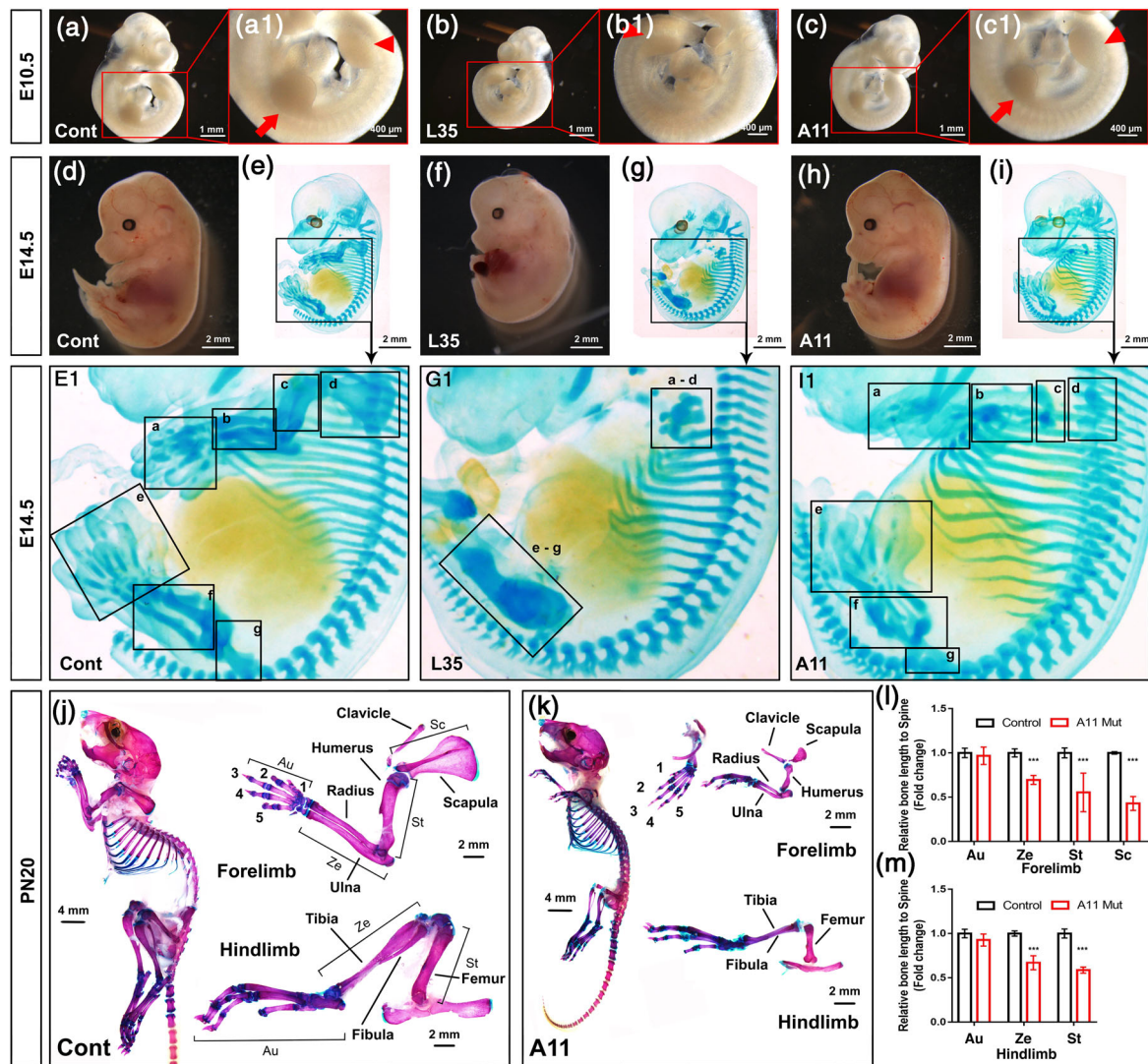
FIGURE 6 Different limb phenotypes in L35 and A11 mouse lines driven by *Prrx1-Cre*. Both line L35 and A11 were bred with the *Prrx1*-Cre mouse line and embryos were harvested at the stages indicated. Skeletal patterns in limbs were visualized either by whole mount cartilage staining (E14.5) or Alcian blue/alizarin red staining (PN20). Bar = 400 μm (A1, B1, C1), 1 mm (A, B, C), or 2 mm (D–I, J, K). For PN20, the length of each segment of limbs are normalized by length of the spine (from cervical 1 to sacral 4) and compared between two genotypes (6 l, m). Au, autopod, Ze, zeugopod, St, stylopod, Sc, scapula. N = 3. ***, p < .001

the length of spine (from cervical 1 to sacral 4) and compared between genotypes. The zeugopods, stylopods and scapulae of A11 mutant mice were unproportionally shorter than those in controls while the autopods were less affected (Figure 6L,M).

The line L35 *caAcvr1* mice have been used as the first genetic mouse model for heterotopic ossification (HO) (Agarwal et al., 2016; Shimono et al., 2011; Valer et al., 2019; Wang et al., 2016; Yu et al., 2008). Standard protocol for HO formation is to locally inject recombinant adenovirus expressing Cre recombinase to increase BMP signaling along with cardiotoxin for local tissue injury (Pan et al., 2020), however, this protocol failed to induce HO in line A11 mice (data not shown). Recently, we reported that breeding with *NFATc1-Cre* mice develop HO without trauma or tissue injury (Agarwal et al., 2015). At PN10, L35 mice carrying *NFATc1-Cre* transgene developed HO around the ankle joint as expected (Figure 7b,b1), while there is no sign of HO

formation in A11 mice carrying *NFATc1-Cre* transgene at PN7 (data not shown) or PN10 (Figure 7c,c1). We also injected cardiotoxin locally into A11 mice carrying *NFATc1-Cre* transgene at PN3, 6 and 9 to induce tissue injury expecting to prompt HO formation, however, there was no signs of HO at PN17 (Figure 7d,e).

In conclusion, the newly generated *ca-Acvr1* line A11 model offers an additional model to understand context-dependent function of BMP-Smad signaling during embryogenesis and after birth. Conditional activation of BMP-Smad signaling can avoid early embryonic lethality caused by ubiquitously increased BMP signaling (Fukuda et al., 2006; Hu et al., 2004). By crossing with three different Cre lines, line A11 mutants show distinct phenotypes from line L35, which we previously reported (Fukuda et al., 2006). There would be several explanations for distinct phenotypes between the two lines generated using the same construct. One is the levels of BMP-Smad signaling. Despite higher
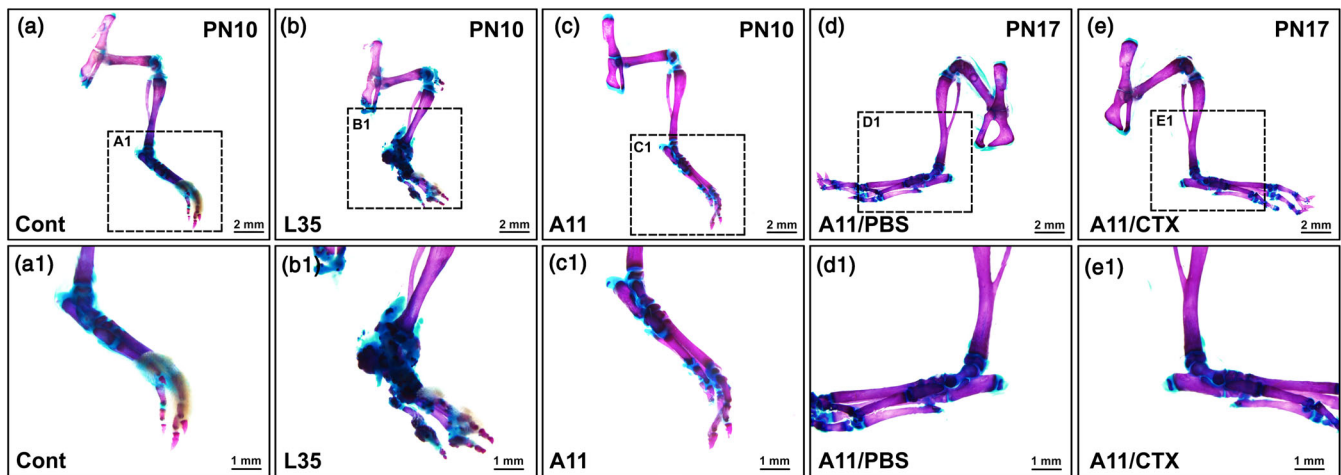
FIGURE 7 Line A11 does not generate heterotopic bones. Both line L35 and A11 were bred with the *NFATc1*-Cre mouse line and formation of heterotopic ossification was assessed at PN10. A11 mice also carrying the *NFATc1*-Cre transgene were treated with cardiotoxin (CTX) to induce tissue injury and formation of heterotopic ossification was assessed at PN17. Bar = 2 mm (a–e) or 1 mm (a1–e1)

copy number of the transgene in line A11, levels of Smad signaling after Cre recombination is lower than that of L35 as shown in Figure 2d. Another speculation is the difference in cell types that express the transgene. Despite our attempts to achieve ubiquitous and strong expression of the transgenes by employing the CAG promoter, expression levels of the transgene are low and restricted for L35 (Fukuda et al., 2006) or under detection for A11. We speculate that the transgene in line L35 is expressed in cells including progenitor and/or multipotent population such as neural crest cells and fibro adipogenic progenitor cells, and thus ectopic cartilage and ectopic bones are developed after Cre recombination (Agarwal et al., 2016; Shimono et al., 2011; Valer et al., 2019; Wang et al., 2016; Yang et al., 2021; Yu et al., 2008). In contrast, the transgene in line A11 may be expressed in committed and or more differentiated cells.

For the potential molecular mechanisms of ectopic cartilage formation found in L35 mut embryos, we recently demonstrated that increased BMP signaling suppresses autophagic activity to lower degradation of β-catenin (Yang et al., 2021). Unlike progenitor cells in limb mesenchyme, reduction in Wnt canonical signaling prompt chondrogenic differentiation of cranial neural crest cells (Yang et al., 2021). Based on the timing of a requirement of Wnt signaling, we speculate that formation of ectopic cartilage is due to aberrant cell fate specification of multipotent population rather than prompting chondrogenesis after lineage commitment (Yang et al., 2021). Taken together with the data that we did not see formation of HO in A11 mut but unproportionally shorter bones in limb, the newly developed line A11 would be suitable to investigate functions of BMP signaling in committed cells for their proliferation, differentiation, migration, and/or cell death.

We previously generated conditional constitutively activated *Bmpr1a* mice, which generate BMP type 1A receptor with a Q233G mutation, using the same transgenic vector (Komatsu et al., 2013). When crossed with *P0-Cre* mice, *ca-Bmpr1a* mice develop skull deformity due to the premature fusion of cranial sutures while the mutant mice can survive over 1 year (Hayano et al., 2015; Komatsu et al., 2013; Pan et al., 2017). Another neural crest conditional *ca-Bmpr1a* mice developed by another group displays ectopic cartilage formation in craniofacial region along with perinatal lethality (Li et al., 2013). It would be an interesting future endeavor to examine the levels and patterns of phospho-Smad1/5/9 among those gain-of-function mutant mice for BMP-Smad signaling to understand highly context-dependent BMP functions.

AUTHOR CONTRIBUTION

Study design: Jingwen Yang, Masako Toda Nakamura and Yuji Mishina. Materials to generate: Tomokazu Fukuda, Yoshihiro Komatsu, and Yuji Mishina. Study conduct: Data collection: Data analysis: Jingwen Yang, Masako Toda Nakamura, Shawn A. Hallett, Hiroki Ueharu, Honghao Zhang, Kristen Kelley. Data interpretation: Jingwen Yang, Masako Toda Nakamura, Hiroki Ueharu, and Yuji Mishina. Writing manuscript: Jingwen Yang and Yuji Mishina. Approving final version of manuscript: Jingwen Yang, Masako Toda Nakamura, Shawn A. Hallett, Hiroki Ueharu, Honghao Zhang, Kristen Kelley, Tomokazu Fukuda, Yoshihiro Komatsu and Yuji Mishina. Jingwen Yang and Yuji Mishina take responsibility for the integrity of the data analysis.

DATA AVAILABILITY STATEMENT

ORCID

Yuji Mishina https://orcid.org/0000-0002-6268-4204

REFERENCES

Agarwal, S., Loder, S., Brownley, C., Cholok, D., Mangiavini, L., Li, J., ... Levi, B. (2016). Inhibition of Hif1alpha prevents both trauma-induced and genetic heterotopic ossification. *Proceedings of the National Academy of Sciences of the United States of America*, 113, E338–E347.

Agarwal, S., Loder, S. J., Brownley, C., Eboda, O., Peterson, J. R., Hayano, S., ... Levi, B. (2015). BMP signaling mediated by constitutively active Activin type 1 receptor (ACVR1) results in ectopic bone formation localized to distal extremity joints. *Developmental Biology*, 400, 202–209.

Bagarova, J., Vonner, A. J., Armstrong, K. A., Borgermann, J., Lai, C. S., Deng, D. Y., ... Yu, P. B. (2013). Constitutively active ALK2 receptor mutants require type II receptor cooperation. *Molecular and Cellular Biology*, 33, 2413–2424.

Brazil, D. P., Church, R. H., Surae, S., Godson, C., & Martin, F. (2015). BMP signalling: Agony and antagony in the family. *Trends in Cell Biology*, 25, 249–264.

Chen, G., Ishan, M., Yang, J., Kishigami, S., Fukuda, T., Scott, G., ... Liu, H. X. (2017). Specific and spatial labeling of P0-Cre versus Wnt1-Cre in cranial neural crest in early mouse embryos. *Genesis*, 55, e23034.

da Silva Madaleno, C., Jatzlau, J., & Knaus, P. (2020). BMP signalling in a mechanical context - implications for bone biology. *Bone*, 137, 115416.

Dudas, M., Sridurongrit, S., Nagy, A., Okazaki, K., & Kaartinen, V. (2004). Craniofacial defects in mice lacking BMP type I receptor Alk2 in neural crest cells. *Mechanisms of Development*, 121, 173–182.

Fukuda, T., Mishina, Y., Walker, M. P., & DiAugustine, R. P. (2005). Conditional transgenic system for mouse aurora a kinase: Degradation by the ubiquitin proteasome pathway controls the level of the transgenic protein. *Molecular and Cellular Biology*, 25, 5270–5281.

Fukuda, T., Scott, G., Komatsu, Y., Araya, R., Kawano, M., Ray, M. K., ... Mishina, Y. (2006). Generation of a mouse with conditionally activated signaling through the BMP receptor, ALK2. *Genesis*, 44, 159–167.

Grafe, I., Alexander, S., Peterson, J. R., Snider, T. N., Levi, B., Lee, B., & Mishina, Y. (2018). TGF-beta family signaling in mesenchymal differentiation. *Cold Spring Harbor Perspectives in Biology*, 10, 717–765.

Gu, Z., Reynolds, E. M., Song, J., Lei, H., Feijen, A., Yu, L., ... Li, E. (1999). The type I serine/threonine kinase receptor ActRIA (ALK2) is required for gastrulation of the mouse embryo. *Development*, 126, 2551–2561.

Hayano, S., Komatsu, Y., Pan, H., & Mishina, Y. (2015). Augmented BMP signaling in the neural crest inhibits nasal cartilage morphogenesis by inducing p53-mediated apoptosis. *Development*, 142, 1357–1367.

Hu, Q., Ueno, N., & Behringer, R. R. (2004). Restriction of BMP4 activity domains in the developing neural tube of the mouse embryo. *EMBO Reports*, 5, 734–739.

Jegalian, B. G., & De Robertis, E. M. (1992). Homeotic transformations in the mouse induced by overexpression of a human Hox3.3 transgene. *Cell*, 71, 901–910.

Jiang, X., Rowitch, D. H., Soriano, P., McMahon, A. P., & Sucov, H. M. (2000). Fate of the mammalian cardiac neural crest. *Development*, 127, 1607–1616.

Kaartinen, V., Dudas, M., Nagy, A., Sridurongrit, S., Lu, M. M., & Epstein, J. A. (2004). Cardiac outflow tract defects in mice lacking ALK2 in neural crest cells. *Development*, 131, 3481–3490.

Kamiya, N., Kaartinen, V. M., & Mishina, Y. (2011). Loss-of-function of ACVR1 in osteoblasts increases bone mass and activates canonical Wnt signaling through suppression of Wnt inhibitors SOST and DKK1. *Biochemical and Biophysical Research Communications*, 414, 326–330.

Kishigami, S., Yoshikawa, S., Castranio, T., Okazaki, K., Furuta, Y., & Mishina, Y. (2004). BMP signaling through ACVRI is required for left-right patterning in the early mouse embryo. *Developmental Biology*, 276, 185–193.

Klingensmith, J., Matsui, M., Yang, Y. P., & Anderson, R. M. (2010). Roles of bone morphogenetic protein signaling and its antagonism in holoprosencephaly. *American Journal of Medical Genetics. Part C, Seminars in Medical Genetics*, 154C, 43–51.

Komatsu, Y., Kaartinen, V., & Mishina, Y. (2011). Cell cycle arrest in node cells governs ciliogenesis at the node to break left-right symmetry. *Development*, 138, 3915–3920.

Komatsu, Y., Yu, P. B., Kamiya, N., Pan, H., Fukuda, T., Scott, G. J., ... Mishina, Y. (2013). Augmentation of Smad-dependent BMP signaling in neural crest cells causes craniosynostosis in mice. *Journal of Bone and Mineral Research*, 28, 1422–1433.

Li, L., Wang, Y., Lin, M., Yuan, G., Yang, G., Zheng, Y., & Chen, Y. (2013). Augmented BMPRIA-mediated BMP signaling in cranial neural crest lineage leads to cleft palate formation and delayed tooth differentiation. *PLoS One*, 8, e66107.

Liu, X., Hayano, S., Pan, H., Inagaki, M., Ninomiya-Tsuji, J., Sun, H., & Mishina, Y. (2018). Compound mutations in Bmpr1a and Tak1 synergize facial deformities via increased cell death. *Genesis*, 56, e23093.

Logan, M., Martin, J. F., Nagy, A., Lobe, C., Olson, E. N., & Tabin, C. J. (2002). Expression of Cre Recombinase in the developing mouse limb bud driven by a Prxl enhancer. *Genesis*, 33, 77–80.

Marchuk, D., Drumm, M., Saulino, A., & Collins, F. S. (1991). Construction of T-vectors, a rapid and general system for direct cloning of unmodified PCR products. *Nucleic Acids Research*, 19, 1154.

Mishina, Y., Crombie, R., Bradley, A., & Behringer, R. R. (1999). Multiple roles for activin-like kinase-2 signaling during mouse embryogenesis. *Developmental Biology*, 213, 314–326.

Morikawa, Y., Zehir, A., Maska, E., Deng, C., Schneider, M. D., Mishina, Y., & Cserjesi, P. (2009). BMP signaling regulates sympathetic nervous system development through Smad4-dependent and -independent pathways. *Development*, 136, 3575–3584.

Muzumdar, M. D., Tasic, B., Miyamichi, K., Li, L., & Luo, L. (2007). A global double-fluorescent Cre reporter mouse. *Genesis*, 45, 593–605.

Noda, K., Mishina, Y., & Komatsu, Y. (2016). Constitutively active mutation of ACVR1 in oral epithelium causes submucous cleft palate in mice. *Developmental Biology*, 415, 306–313.

Nomura-Kitabayashi, A., Phoon, C. K., Kishigami, S., Rosenthal, J., Yamauchi, Y., Abe, K., ... Mishina, Y. (2009). Outflow tract cushions perform a critical valve-like function in the early embryonic heart requiring BMPRIA-mediated signaling in cardiac neural crest. *American Journal of Physiology. Heart and Circulatory Physiology*, 297, H1617–H1628.

Pan, H., Fleming, N., Hong, C. C., Mishina, Y., & Perrien, D. S. (2020). Methods for the reliable induction of heterotopic ossification in the conditional Alk2(Q207D) mouse. *Journal of Musculoskeletal & Neuronal Interactions*, 20, 149–159.

Pan, H., Zhang, H., Abraham, P., Komatsu, Y., Lyons, K., Kaartinen, V., & Mishina, Y. (2017). BmpR1A is a major type 1 BMP receptor for BMP-Smad signaling during skull development. *Developmental Biology*, 429, 260–270.

Sampath, T. K., & Reddi, A. H. (2020). Discovery of bone morphogenetic proteins - A historical perspective. *Bone*, 140, 115548.

Sanchez-Duffhues, G., Williams, E., Goumans, M. J., Heldin, C. H., & Ten Dijke, P. (2020). Bone morphogenetic protein receptors: Structure, function and targeting by selective small molecule kinase inhibitors. *Bone*, 138, 115472.

Shi, C., Mandair, G. S., Zhang, H., Vanrenterghem, G. G., Ridella, R., Takahashi, A., … Sun, H. (2018). Bone morphogenetic protein signaling through ACVR1 and BMPR1A negatively regulates bone mass along with alterations in bone composition. *Journal of Structural Biology*, *201*, 237–246.

Shimono, K., Tung, W. E., Macolino, C., Chi, A. H., Didizian, J. H., Mundy, C., … Iwamoto, M. (2011). Potent inhibition of heterotopic ossification by nuclear retinoic acid receptor-gamma agonists. *Nature Medicine*, *17*, 454–460.

Shore, E. M., Xu, M., Feldman, G. J., Fenstermacher, D. A., Cho, T. J., Choi, I. H., … Kaplan, F. S. (2006). A recurrent mutation in the BMP type I receptor ACVR1 causes inherited and sporadic fibrodysplasia ossificans progressiva. *Nature Genetics*, *38*, 525–527.

Stottmann, R. W., Choi, M., Mishina, Y., Meyers, E. N., & Klingensmith, J. (2004). BMP receptor IA is required in mammalian neural crest cells for development of the cardiac outflow tract and ventricular myocardium. *Development*, *131*, 2205–2218.

Suzawa, T., Yoshida, H., Takahashi, M., Itose, M., Takimoto, R., Sasama, Y., … Kamijo, R. (2020). Prospects of neural crest-derived cells from oral and dentofacial tissues for application in regenerative medicine. *Oral Science International*, *17*, 115–124.

Valer, J. A., Sanchez-de-Diego, C., Gamez, B., Mishina, Y., Rosa, J. L., & Ventura, F. (2019). Inhibition of phosphatidylinositol 3-kinase alpha (PI3Kalpha) prevents heterotopic ossification. *EMBO Molecular Medicine*, *11*, e10567.

Wang, H., Lindborg, C., Lounev, V., Kim, J. H., McCarrick-Walmsley, R., Xu, M., … Pignolo, R. J. (2016). Cellular hypoxia promotes heterotopic ossification by amplifying BMP signaling. *Journal of Bone and Mineral Research*, *31*, 1652–1665.

Wrana, J. L., Attisano, L., Wieser, R., Ventura, F., & Massague, J. (1994). Mechanism of activation of the TGF-beta receptor. *Nature*, *370*, 341–347.

Wu, B., Zhang, Z., Lui, W., Chen, X., Wang, Y., Chamberlain, A. A., … Zhou, B. (2012). Endocardial cells form the coronary arteries by angiogenesis through myocardial-endocardial VEGF signaling. *Cell*, *151*, 1083–1096.

Yamauchi, Y., Abe, K., Mantani, A., Hitoshi, Y., Suzuki, M., Osuzu, F., … Yamamura, K. (1999). A novel transgenic technique that allows specific marking of the neural crest cell lineage in mice. *Developmental Biology*, *212*, 191–203.

Yang, J., Kitami, M., Pan, H., Nakamura, M. T., Zhang, H., Liu, F., … Mishina, Y. (2021). Augmented BMP signaling commits cranial neural crest cells to a chondrogenic fate by suppressing autophagic beta-catenin degradation. *Science Signaling*, *14*, eaaz9368.

Yang, J., & Mishina, Y. (2019). Generation and identification of genetically modified mice for BMP receptors. *Methods in Molecular Biology*, *1891*, 165–177.

Yang, J., Ueharu, H., & Mishina, Y. (2020). Energy metabolism: A newly emerging target of BMP signaling in bone homeostasis. *Bone*, *138*, 115467.

Yu, P. B., Deng, D. Y., Lai, C. S., Hong, C. C., Cuny, G. D., Bouxsein, M. L., … Bloch, K. D. (2008). BMP type I receptor inhibition reduces heterotopic ossification. *Nature Medicine*, *14*, 1363–1369.

Zhang, H., Takeda, H., Tsuji, T., Kamiya, N., Rajderkar, S., Louie, K., … Mishina, Y. (2015). Generation of Evc2/Limbin global and conditional KO mice and its roles during mineralized tissue formation. *Genesis*, *53*, 612–626.

Zhao, G. Q. (2003). Consequences of knocking out BMP signaling in the mouse. *Genesis*, *35*, 43–56.

SUPPORTING INFORMATION

Additional supporting information may be found online in the Supporting Information section at the end of this article.